Geophysical Research Letters

RESEARCH LETTER
10.1029/2023GL102928

Directly Dating Plio-Pleistocene Climate Change in the Terrestrial Record

Maximilian Dröllner[1], Milo Barham[1], Christopher L. Kirkland[1], Martin Danišík[2], Julien Bourdet[3], Maike Schulz[4], and Mehrooz Aspandiar[5]

[1]Timescales of Mineral Systems Group, School of Earth and Planetary Sciences, Curtin University, Perth, WA, Australia, [2]John de Laeter Centre (JdLC), Curtin University, Perth, WA, Australia, [3]CSIRO Energy Resources, Australian Resources Research Centre, Kensington, WA, Australia, [4]Institut für Geologie und Paläontologie, Westfälische Wilhelms-Universität, Münster, Germany, [5]School of Earth and Planetary Sciences, Curtin University, Perth, WA, Australia

Abstract Accurate chronology of climatic shifts is critical to understand the controls on landscape and species evolution. Unfortunately, direct dating of continental climate change is hindered by the scarcity of dateable terrestrial products evidencing climatic shifts. Here we use ferruginous indurations from the arid landscapes of the Nullarbor Plain in southern Australia to constrain the timing of Plio-Pleistocene aridification in the continental realm. We present (U-Th)/He goethite data implying active induration processes between c. 2.7 and 2.4 Ma. Chemical-mineralogical and petrographic examination suggests that formation of ferruginous indurations was linked with a decline of the groundwater table, driven by the rapid climatic shift from humid late Pliocene to arid early Pleistocene conditions. Combined with local to global climatic proxies, we conclude that ferruginous indurations are promising targets to obtain absolute ages on landscape evolution to refine continental climatic chronology and improve understanding of the environmental drivers of species diversification and extinction.

Plain Language Summary The reconstruction of Earth's climate record is typically founded on the physicochemical properties of marine sediments. Continental sediments that yield time-constrained climate information are rare, but important to interpret wider Earth system responses and the co-evolution of regional climate, landscape, and biota. This study presents direct dating of continental climate change on the Nullarbor Plain to constrain its development as an important biogeographic barrier driving species diversification between SW- and SE-Australia. Age dating of iron-oxide cements constrains the waning availability of mobile water (e.g., groundwater) and the onset of drier conditions related to global Plio-Pleistocene climate change. These findings demonstrate that iron-oxides may provide an excellent continental archive to anchor major climate shifts and help understand associated terrestrial ecosystem change.

Key Points:

- (U-Th)/He data from ferruginous indurations capture the onset of Plio-Pleistocene aridification in southern Australia
- Correlation of induration age with other climatic proxies indicates that ferruginous indurations track terrestrial water table evolution
- Timing of aridification constrains evolution of important biogeographic barrier

Supporting Information:

Supporting Information may be found in the online version of this article.

Correspondence to:

M. Dröllner,
maximilian.drollner@curtin.edu.au

Citation:

Dröllner, M., Barham, M., Kirkland, C. L., Danišík, M., Bourdet, J., Schulz, M., & Aspandiar, M. (2023). Directly dating Plio-Pleistocene climate change in the terrestrial record. *Geophysical Research Letters*, *50*, e2023GL102928. https://doi.org/10.1029/2023GL102928

Received 30 JAN 2023
Accepted 20 MAR 2023

Author Contributions:

Conceptualization: Maximilian Dröllner, Milo Barham, Christopher L. Kirkland, Martin Danišík
Formal analysis: Maximilian Dröllner, Martin Danišík, Julien Bourdet, Maike Schulz
Funding acquisition: Milo Barham, Christopher L. Kirkland
Investigation: Maximilian Dröllner, Milo Barham, Christopher L. Kirkland, Martin Danišík, Maike Schulz, Mehrooz Aspandiar
Methodology: Maximilian Dröllner, Martin Danišík, Julien Bourdet, Maike Schulz

1. Introduction

The Plio–Pleistocene witnessed a major shift of the global climate (Balco & Rovey, 2010; Hill et al., 2017; Lisiecki & Raymo, 2007), with significant expansion of northern hemisphere glaciation (Bailey et al., 2013; Haug et al., 1999) driving a change from a wet and humid state during the Pliocene, to colder and more arid conditions in the Pleistocene (Filippelli & Flores, 2009). This climate change had profound impacts on Earth's ecosystems: vast areas of dense forests were replaced by more open vegetation (e.g., grasslands) prompting habitat reorganization and possibly strongly influencing hominin evolution (DeMenocal, 2011; Reed, 1997; Trauth et al., 2021). Despite the undoubted significance of this event, constraining the timing of continental environmental response to climate change is complicated by the discontinuous continental sediment record and challenges of absolute dating geological processes that can be clearly linked to environmental perturbation. These difficulties have hampered the direct dating of Plio–Pleistocene transition processes in the continental realm, with studies instead often relying on marine depositional records to reconstruct continental paleoclimate (Christensen et al., 2017; Lisiecki & Raymo, 2007; Petrick et al., 2019).

In Australia (Figure 1), declining rainfall, continental moisture, and sea surface temperatures, as well as increasing dust transport are recorded in marine sediment proxies deposited during the Plio-Pleistocene transition (de Vleeschouwer et al., 2019; He et al., 2021; Petrick et al., 2019) (Figure 1c). This climate archive, and broadly coeval changes of continental landscapes, such as the initiation of desert dune fields (Fujioka et al., 2009),

Project Administration: Milo Barham, Christopher L. Kirkland
Resources: Milo Barham
Supervision: Milo Barham, Christopher L. Kirkland, Martin Danišík
Validation: Maximilian Dröllner, Milo Barham, Christopher L. Kirkland, Martin Danišík, Julien Bourdet, Mehrooz Aspandiar
Visualization: Maximilian Dröllner
Writing – original draft: Maximilian Dröllner
Writing – review & editing: Maximilian Dröllner, Milo Barham, Christopher L. Kirkland, Martin Danišík, Julien Bourdet, Maike Schulz, Mehrooz Aspandiar

are consistent with aridification of Australia's continental climate. The vast expanses of the Nullarbor Plain in south-central Australia (Figure 1) which covers about 200,000 km^2 of treeless shrublands, is devoid of any surface water features. The Nullarbor Plain represents the modern manifestation of the Plio-Pleistocene shift to extensive dryland areas, which now cover ∼46% of Earth's land surface, and host ∼3 billion people (Mirzabaev et al., 2019; van der Esch et al., 2017). Increasing aridity on the Nullarbor Plain is tracked through the decline of speleothem development as a consequence of reduced continental moisture, pedogenic calcrete and the lowering of the groundwater table (Lipar & Ferk, 2015; C. R. Miller et al., 2012; Woodhead et al., 2019). Similarly, drier climate in Australia in the Pleistocene is linked with the retreat of (rain)forests in favor of open wood- and grassland vegetation (Martin, 2006). Such extensive changes in climate and vegetation created new habitats, but also established biogeographic barriers, both of which significantly influenced partitioning and diversification across Australia's biota (Ansari et al., 2019; Byrne et al., 2008; Pepper & Keogh, 2021). Among other examples, sister species of birds (White et al., 2011), insects (Owen et al., 2017), and plants (Crisp & Cook, 2007) reside in Australia's SW and SE temperate biomes, separated by the arid Nullarbor Plain (Figures 1a and 1b).

Despite the significance of the Plio-Pleistocene transition, the absolute timing of changes in the continental record of aridification on the Nullarbor Plain remains poorly constrained (C. R. Miller et al., 2012), impeding integration of local paleoclimate indicators into regional, and ultimately global models. A compelling target to improve terrestrial climate models is iron oxides, which form at a broad range of surface conditions (Bigham et al., 2002), often in relation to environmental changes (Zhao et al., 2017). Goethite is the most abundant Earth surface iron oxide (*sensu lato*) and occurs in many environments (Schwertmann & Taylor, 1989). In arid environments, goethite can be generated in response to a lowering of the water table and hence, can trace hydrological changes due to aridification (Heim et al., 2006). Hence, environmental information is recorded by temporal constraints on iron oxide formation and can provide direct insights into landscape evolution, in turn informing on biogeographic models (Gautheron et al., 2022). Here, we use (U-Th)/He geochronology, mineralogy, and geochemistry applied to diagenetic ferruginous indurations, hosted in Eocene-Miocene paleo-shoreline deposits in southern Australia, to better constrain the chronology of aridification of the Nullarbor Plain. We further demonstrate the broader importance of dating indurations for understanding landscape evolution and biogeography.

2. Materials and Methods

This study examined iron oxides from a ferruginous induration from the Jacinth-Ambrosia heavy mineral sand deposit (30° 54′ 33.84″ S, 132° 13′ 5.88″ E). Here, active open pit mining provides a unique window into the geological history of the extensive paleo-shoreline deposits fringing the Nullarbor Plain. The stratigraphy of the Jacinth-Ambrosia deposit (Figure 1f) was established by Hou et al. (2011). At the study site, diagenetic iron oxides (and -hydroxides) form ferruginous indurations overprinting the shallow marine middle-upper Eocene Ooldea Sands that overlie weathered granitic basement and underlie reworked Miocene sands. Samples were taken from cross-bedded sands (Figure 1d) at the base of the mine pit (c. 25–30 m below the surface and c. 2 m above bedrock), where Ooldea Sands are strongly indurated in comparison to less prominent indurations in overlying strata. Macroscopically, the sampled indurations (Figure 1e) are (a) well-consolidated reddish fine- to coarse-grained sandstones, (b) display veins of metallic to vitreous luster with rare mineral inclusions, and (c) contain mm- to cm- sized cavities, which document secondary partial or complete infills of various compositions (clay- to sand-sized particles with variable sorting). From one representative ferruginous induration, several rock slabs (c. 25 × 10 mm) were prepared for further investigation. Sample characterization included use of X-ray powder diffraction (XRD), energy-dispersive spectroscopy (EDS), and Raman spectroscopy (methods are outlined in Texts S1–S3 in the Supporting Information S1 available through https://doi.org/10.5281/zenodo.7739575). (U-Th)/He dating (Text S4 in the Supporting Information S1) followed the analytical procedures in Danišík et al. (2013) and used 100–300 μm large fragments of goethite that were extracted from (a) the veins/cement of metallic to vitreous luster (from the surface of the induration) and (b) the iron-rich domains of argillaceous zoned cutan structures from polished rock slabs. (U-Th)/He measurements are corrected for diffusive loss of He following the recommendations of Bassal et al. (2022).

3. Results

3.1. Ferruginous Induration Characteristics

Mineralogical bulk analysis of the ferruginous induration using XRD (Table S1 in the Supporting Information S1, Table S5, and Figure S2 in the Supporting Information S1) indicates the presence of quartz and heavy minerals

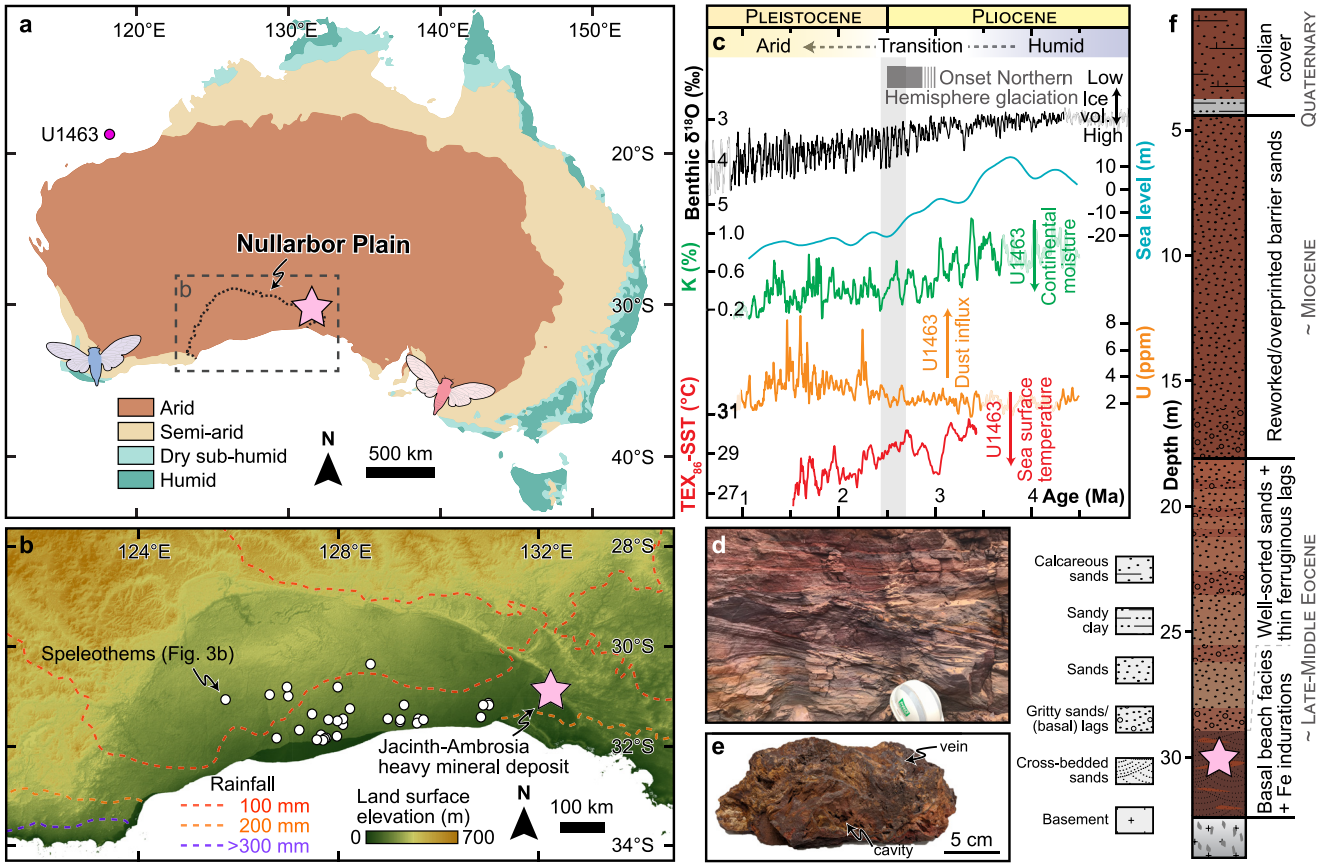

Figure 1. (a) Climatic zonation across Australia based on the Aridity Index (Zomer et al., 2008). Colored insects represent biotic divergence via the distributions of sister species of cicadas *A. dolens* (blue) and *A.* "mallee hisser" (red) that are found in Australia's SW and SE temperate biomes, respectively, separated by the arid Nullarbor Plain (Owen et al., 2017). Pink star and purple circle indicate the sample location and site U1463, respectively (Figure 1c). (b) Digital elevation model of the Nullarbor Plain and isohyets of mean annual rainfall (http://www.bom.gov.au/). (c) Climatic proxies showing (from top to bottom) shift from humid to arid conditions in NW Australia (Christensen et al., 2017), onset of the Northern Hemisphere glaciation (Haug et al., 1999), increasing ice volumes (Lisiecki & Raymo, 2005), smoothed sea level (K. G. Miller et al., 2020), potassium wireline log data at site U1463 (Christensen et al., 2017), uranium wireline log data at site U1463 (Christensen et al., 2017), and sea surface temperatures at site U1463 (Smith et al., 2020). Gray vertical rectangle in the background is from Figure 3a and denotes the time of formation for the ferruginous indurations in the Ooldea Sands (this study). (d) Jacinth-Ambrosia heavy mineral sand deposit showing iron-rich indurated horizons and cross-bedded sands (white helmet measures 25 cm across). (e) Analyzed ferruginous induration showing targeted structures. (f) Schematic stratigraphy of the Jacinth-Ambrosia deposit (modified after Hou et al., 2011).

(mainly zircon) as the dominant detritus, and moderate proportions (i.e., 1–5 wt%) of goethite (α-FeO(OH)) and hematite (α-Fe_2O_3). Backscattered electron imaging (Figure 2a) and chemical composition mapping by EDS (Figure 2b) of polished rock slabs from the indurations suggest that fine-grained infills of clay and iron-rich domains of cement (corresponding to veins of metallic to vitreous luster; Figure 2b) comprise iron-rich polycrystalline mineral aggregates with traces of silicon and alumina (Figure 2c). While depositional sedimentary structures, such as the segregation of dense and light minerals, are preserved, other petrographic characteristics indicate scarce remnants of pedogenetic processes. Specifically, the fine-grained infills, identified as argillaceous zoned cutan structures, indicate replacement of primary material (e.g., roots or burrows) by illuviated clay infills that underwent secondary geochemical alteration initiating chemical zonation (Nahon, 1991a; Salama et al., 2022). This chemical trend is manifested by increasing iron and decreasing silicon contents toward the rim of the cutan structures (Figure 2c). Iron oxide domains sampled for geochronological analysis (selected based on low impurities documented by light and electron miscopy) predominantly consist of goethite based on Raman spectroscopy (Figure 2d).

3.2. Geochronological Results

In total, 19 mechanically extracted goethite-bearing fragments from the vein/cement (Figure 1e, Figures S1a–S1c in the Supporting Information S1) and cutan structures (Figures 2a and S1e in the Supporting Information S1)

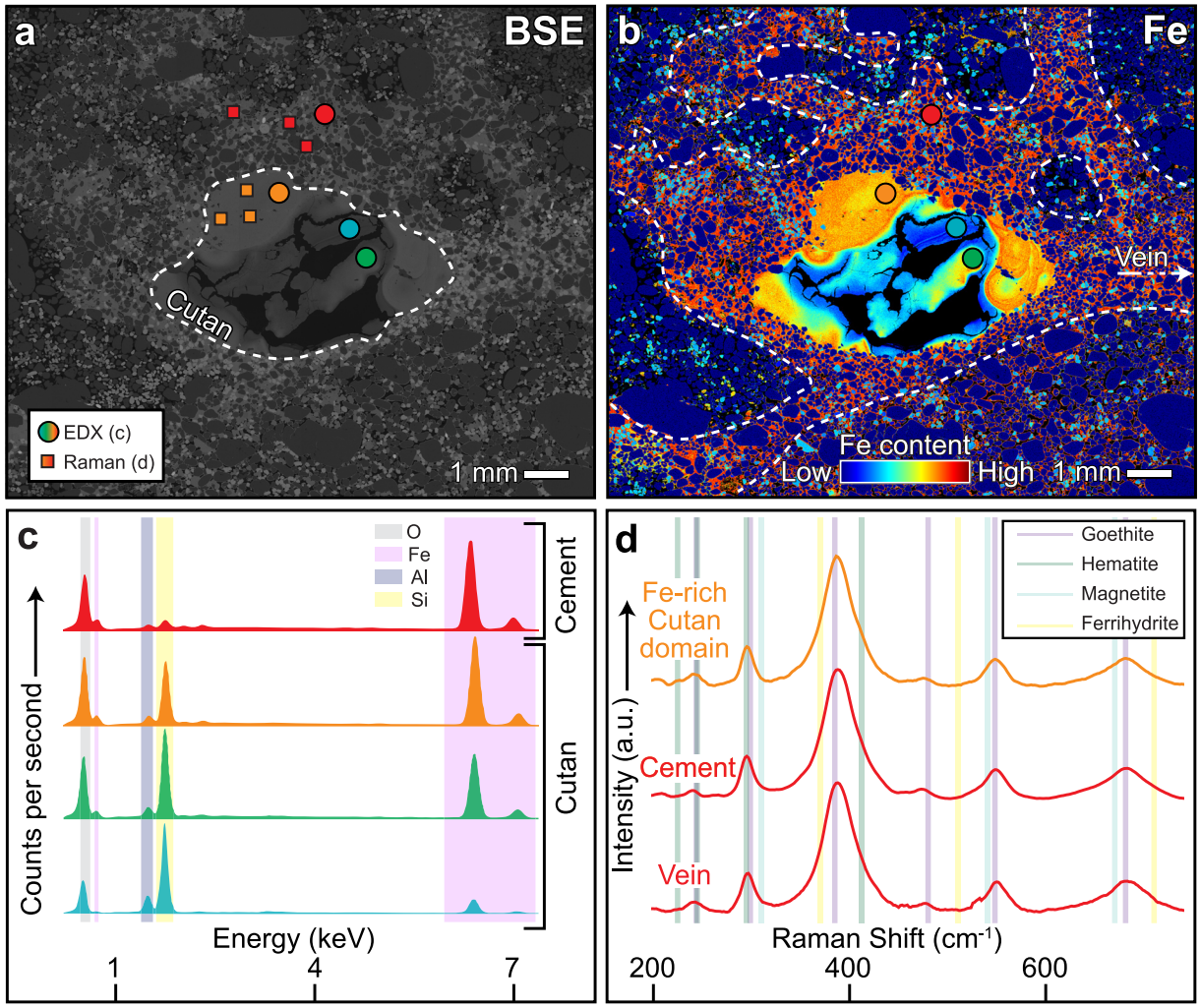

Figure 2. (a) Backscattered electron image of a relic pedogenetic structure (cutan). Circle and squares denote locations of representative spot analyses using energy-dispersive spectroscopy (EDS) and Raman spectroscopy, respectively, to demonstrate chemical and mineralogical trends (colors corresponds to spectra in Figure 2c). (b) Iron content for the same sample extent. Dashed lines indicate areas of iron-rich cement domains, which macroscopically correspond to veins of metallic to vitreous luster (indicated by white arrow). (c) Representative EDS spectra for different domains demonstrating increase of iron (and decrease of alumina and silicon) toward the outer domains of the cutan structure. Vertical colored rectangles show characteristic energy levels of relevant elements. (d) Raman spectra of different domains (a.u. = arbitrary units). Individual analyses (Table S4) within each domain (i.e., cutan, cement, and vein) are highly similar and, thus, were averaged. Spectra are shown as 5-point running average and are baseline subtracted using a convex hull fit. Vertical lines show diagnostic Raman shift values (Hanesch, 2009).

were analyzed. (U-Th)/He isotopic measurements yield thermochronological median dates for cutan and vein/cement structures of 2.4 ± 0.7 Ma (1 standard deviation, 1 SD) and 2.7 ± 0.8 Ma (1 SD), respectively (Table S2 in the Supporting Information S1). An Epps–Singleton (Epps & Singleton, 1986) test for equal distributions applying a small sample correction (W2 = 3.3; p = 0.5) implies distributions of cutan and vein/cement dates are statistically indistinguishable. Based on the indistinguishable median dates and identical mineralogy (all fragments are goethite), cutan and vein/cement fragments are considered to represent a single age population reflecting a contemporaneous response to a shared geological process. Consequently, an uncertainty-weighted mean of 2.56 ± 0.13 Ma (2 standard error, 2 SE) is calculated (Figure 3a). Three dates are rejected from the weighted mean calculation based on Chauvenet's criterion for outlier detection (Table S2 in the Supporting Information S1). Statistical rejections are supported by petrographic observations of outliers hosting larger amounts of detrital grains (Figure S1d in the Supporting Information S1). We posit that spuriously old ages reflect He-bearing inclusions (e.g., zircon). Similarly, very young ages (present in cutan analyses) may be associated with alpha-ejection into voids (Danišík et al., 2017) or reflect domains of decreased He retentivity (Shuster et al., 2005). Mean squared weighted deviation above unity (here 2.5) are commonly observed in (U-Th)/He

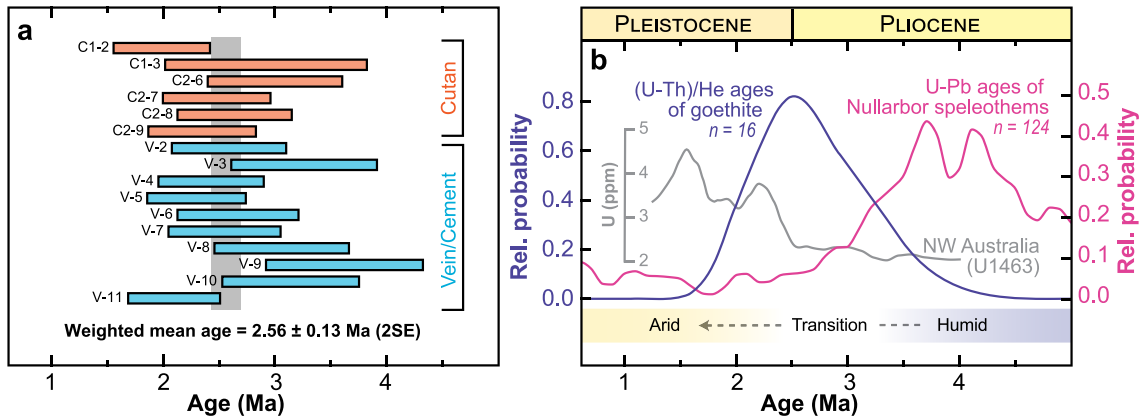

Figure 3. (a) Individual (U-Th)/He ages at 2 SE uncertainty of cutan (orange) and vein/cement (blue) fragments. Gray vertical rectangle in the background denotes the weighted mean age (2 SE). (b) Probability density plot (PDP) of (U-Th)/He ages of goethite compared to PDP of U-Pb ages of speleothems across the Nullarbor Plain (Woodhead et al., 2019) and locally weighted smoothing of the uranium wireline log data at site U1463 as a proxy for continental dust dispersion tracking increasing aridity (Christensen et al., 2017).

thermochronology and do not impede meaningful age determination, but rather convey the degree of complexity in the geological process (Reiners & Nicolescu, 2006). Hence, the 2.56 ± 0.13 Ma age is interpreted as the best estimate of the time of formation for the ferruginous indurations in the Ooldea Sands.

4. Discussion and Conclusions

4.1. Groundwater Decline in Response to Climate Change

Growth of goethite is controlled by environmental conditions, but typically involves oxidation and hydrolysis of dissolved ferrous iron (Fe^{2+}) and is favored by pH values around 3–7 and high water activity (Bigham et al., 2002). Acidic and iron-rich fluids are observed in modern groundwater systems in the study area (Reid et al., 2018), and suggest, in tandem with textural observations (Section 3.1), goethite growth within a meteoric environment as the most likely scenario. Dissolved ferrous iron was plausibly extracted during weathering of lateritic paleosols (Nahon, 1991b) that formed extensively throughout the Oligocene and Miocene (Martin, 2006). This interpretation is supported by the occurrence of pedogenetic relics (e.g., argillaceous cutan, Figures 2a and 2b) and field observations of bleached and mottled sands in overlying sediments (Hou et al., 2011) evidencing iron remobilization, a process likely facilitated during the late Pliocene's humid climate. The subsequent transition to more arid conditions would have led to a lowering of the water table, in turn oxidizing ferrous iron. An oxygenated meteoric environment for the formation of the ferruginous indurations is consistent with the absence of reduced phases (e.g., magnetite, pyrite), the geochemical alteration of the illuviated clay infill along a redox gradient (cutan), and provides high water activity favoring the formation of goethite over hematite. The latter mineral prefers low water activity (Torrent et al., 1982) and may be formed in some rapidly drying parts of the indurations (thus explaining the reddish hue and hematite in the bulk XRD analysis), whereas residual water in larger pores would foster the growth of goethite. The textural and mineralogical observations support a near-surface genesis and suggest that (U-Th)/He ages can provide direct constraints on the formation of ferruginous indurations (Shuster et al., 2005). However, the rate of goethite growth cannot be precisely defined as analytical uncertainty likely exceeds the recorded duration of goethite aggregation (Guyodo et al., 2003; Yee et al., 2006). Hence, we posit that the water table declined within the given uncertainty of the mean (U-Th)/He age that can be interpreted as the time of the formation event (i.e., induration). Hence, conservatively, the geochronological results (Figure 3a) suggest that induration formation in the study area was active between c. 2.7 and 2.4 Ma.

4.2. Implications for Arid Landscape Evolution and Species Diversity

The formation of ferruginous indurations in response to the lowering of groundwater is consistent with other indicators of hydrological changes (e.g., collapse of dissolution cavities, pedogenetic calcrete, and appearance of aeolian quartz; Lipar & Ferk, 2015; C. R. Miller et al., 2012) on the Nullarbor Plain during the Plio-Pleistocene

10.1029/2023GL102928

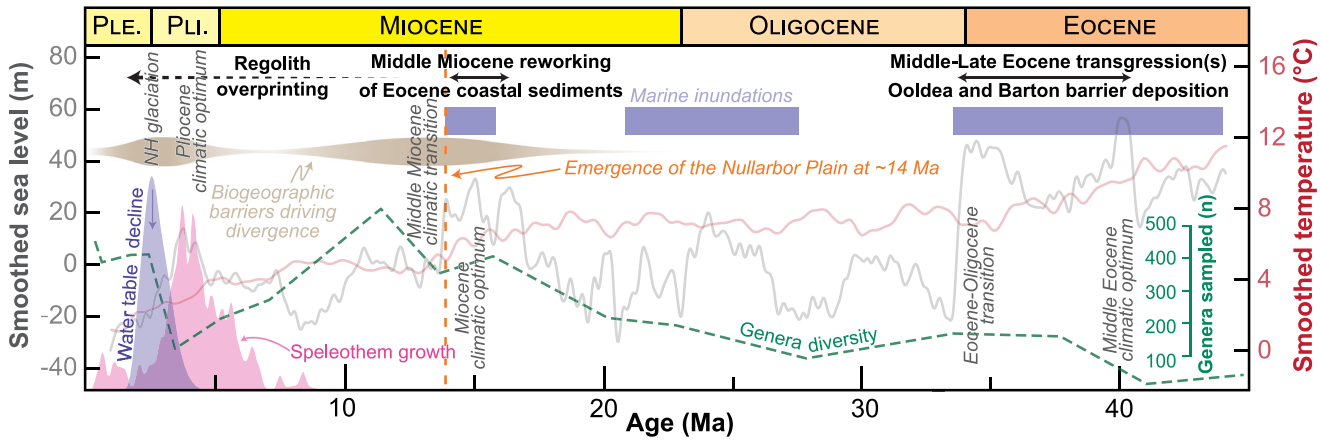

Figure 4. Cenozoic history of the Nullarbor Plain showing geological processes documented in the Ooldea Sands (Hou et al., 2011), major marine indurations (Crisp & Cook, 2007), global sea level (pale gray line; K. G. Miller et al., 2020) and temperatures (pale red line; Cramer et al., 2011). PDPs of late Cenozoic terrestrial products (blue and red areas) are from Figure 3b. Genera diversity (green dashes) of Australia is from the Paleobiology Database (paleobiodb.org) and the interpreted influence of the Nullarbor Plain as a biogeographic barrier on species divergence is shown in brown (Crisp & Cook, 2007; Owen et al., 2017; Rix et al., 2015; White et al., 2011) (wide and thin parts are strong and weak influence, respectively). Emergence at c. 14 Ma (Webb & James, 2006) reflects permanent subaerial exposure of large parts of the Nullarbor Plain. Names of recognized stages of the Cenozoic climate are from K. G. Miller et al. (2020). PLE. - Pleistocene, PLI. - Pliocene.

transition. Woodhead et al. (2019) revealed speleothem growth in shallow caves of the Nullarbor Plain between 5 and 3 Ma that experienced a significant decline after 2.5 Ma (Figure 3b), fingerprinting a rapid decline of mobile water. Importantly, the decline of speleothem formation was broadly coeval with induration formation (Figure 3b), consistent with a major hydrological change toward drier conditions in the Nullarbor Plain. The water table before the Plio-Pleistocene climate change appears to be at least 20 m above the modern (pre-mining) water table (c. 50 m, IGS, 2019). Similar lowering of groundwater levels have been determined for more recent but comparable (i.e., from wet to arid conditions) climate shifts, for example, c. 18 m decline during the last deglaciation at c. 15 ka (Seltzer et al., 2019), suggesting rapid changes of the water table can occur on millennial timescales. Therefore, following a rapid decline and induration formation between 2.7 and 2.4 Ma, the study site's water table at 2.4 Ma may have been comparable to modern conditions without sufficient recharge to reach pre-Pleistocene levels. The high degree of reproducibility in the (U-Th)/He ages is also consistent with negligible disturbance after induration formation. On a larger scale, it appears that the temporal constraints associated with terrestrial formation processes are in excellent agreement with the climatic evolution of Australia's continental interior, which is recorded in the high-resolution and continuous marine deposits of Australia's NW shelf (e.g., Groeneveld et al., 2021; Figure 1a). These marine sediments record the degree of fluvial and windblown terrigenous input and reveal a c. 5.5–3.3 Ma humid interval followed by a transition period foreshadowing the advent of fully arid conditions at c. 2.4 Ma (Christensen et al., 2017). Importantly, windblown terrigenous material derived from large parts of continental Australia (e.g., Courtillat et al., 2020) track aridity, where heightened aridification is fingerprinted by increasing uranium content (a measure of dust activity). Such increase in dust follows the maxima of (U-Th)/He ages at c. 2.6 Ma (Figure 3b). Based on these combined paleoclimate proxies across vast parts of Australia, the formation ages of ferruginous indurations are best explained as marking cessation of humid conditions and imply a minimum constraint of 2.7–2.4 Ma for the emergence of arid-dominated environmental conditions that presently extend over 70% of the Australian continent (Figure 1a). Therefore, geochronological results on targeted induration features document a major turning point in Australia's landscape evolution that has lasted until the present day (Figure 1a).

The Nullarbor Plain's climatic and tectonic history significantly influenced ecosystem changes in Australia throughout the Cenozoic (Figure 4). Following episodes of marine inundation, the Nullarbor Plain became permanently subaerially exposed during the middle Miocene coincident with a climatic transition and shift toward more arid conditions (which was later reversed during the early Pliocene; Sniderman et al., 2016). This period of emergence and drying correlates with a major east-west vicariance of flora and fauna (Rix et al., 2015; White et al., 2011), suggesting the Nullarbor Plain began acting as a significant biogeographic barrier. The Plio-Pleistocene climate shift toward pervasive arid conditions re-established the Nullarbor Plain as a pronounced biogeographic barrier driving ecosystem change by effectively separating mesic environments, resulting in the

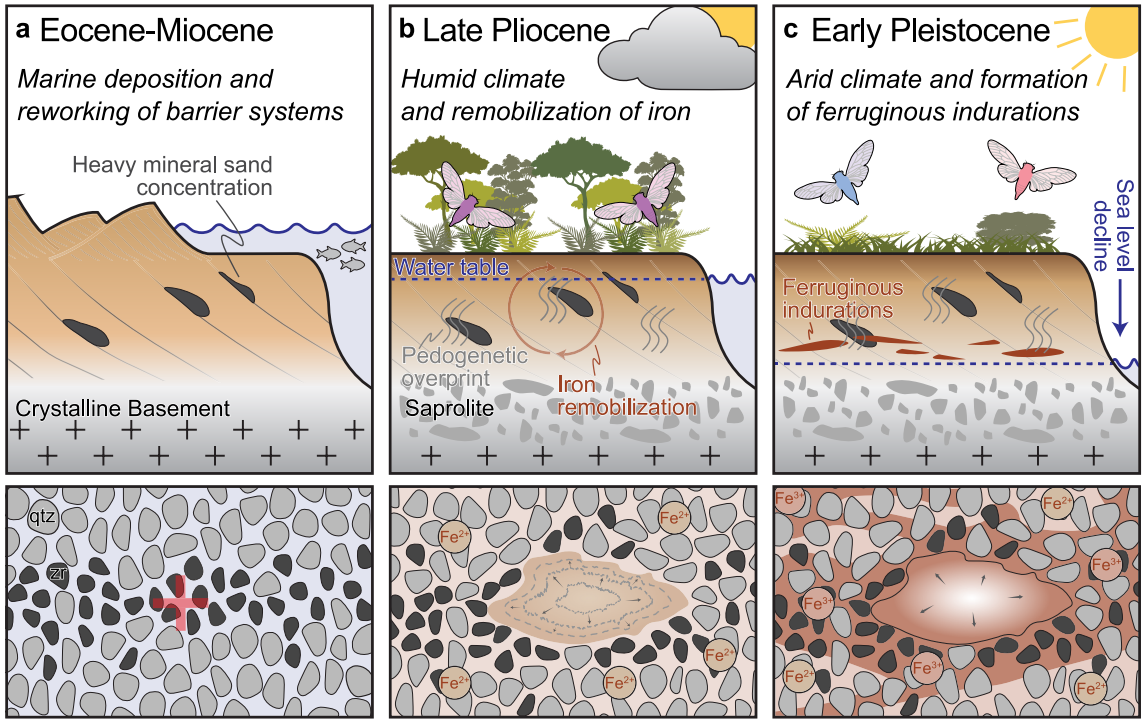

Figure 5. Conceptual model for the ferruginous indurations. The upper panels (top) depict environmental changes and lower panels (bottom) show stages leading to the induration formation. (a) Top: Shallow marine deposition and later reworking (Hou et al., 2011), resulting in heavy mineral concentration, create the substrate that later hosts the indurations. Bottom: Marine sands showing separation processes between light, for example, quartz (qtz), and heavy minerals, for example, zircon (zr). Red cross indicates location of emplacement of textural heterogeneity accommodating cutan growth (b) Top: Late Pliocene humid climate with relatively dense forests and high water table follows episodes of regolith/pedogenetic overprint (Figure 4). Purple cicada reflects a common ancestor inhabiting a continuous mesic habitat (Owen et al., 2017). Bottom: Sand is groundwater-saturated with high concentrations of ferrous iron due to iron remobilization. Geochemical transformation of illuviated clay infill begins forming concentric cutan structures. (c) Top: Rapid climate shift toward the arid early Pleistocene results in water table lowering and the formation of indurations. A decrease of mobile water causes a decline in vegetation that involves the separation of temperate biomes, ultimately favoring the divergence of species. The latter is represented by the blue and red cicadas that diverge from a common ancestor (Figure 5b). Bottom: Higher iron saturation and oxygenated condition in the upper groundwater table oxidize dissolved ferrous to ferric iron that allows build-up of ferruginous indurations.

youngest divergence events (Crisp & Cook, 2007; Owen et al., 2017). The rapid decline of surface water on the Nullarbor Plain led to decreasing vegetation, which in turn directly influenced the distribution and divergence of species because of changes in both food sources and habitat. The temporal consistency of aridification and phylogenetic divergence estimates (Owen et al., 2017; White et al., 2011) supports vicariance models and implies divergence was plausibly driven by the termination of a continuous mesic landscape. Such interpretations are consistent with observations that patterns of high genera diversity either coincide with or follow periods with strong evidence for the Nullarbor Plain acting as a biogeographic barrier (Figure 4).

Integration of petrographic, chemical, and mineralogical observations of ferruginous indurations suggest a polyphase genesis that encompasses (a) initial host sedimentation during middle-late Eocene transgression and middle Miocene reworking (Figure 5a), (b) subsequent regolith overprinting including pedogenetic processes, and (c) a major hydrological change during the Plio-Pleistocene transition. The latter process is manifested through the c. 2.7–2.4 Ma formation of ferruginous indurations, interpreted as a consequence of a rapid shift from the late Pliocene humid climate (Figure 5b) to arid conditions, prevalent since the early Pleistocene (Figure 5c). Overall, the apparent relationship of ferruginous indurations and groundwater decline most likely reflects the terrestrial response to climatic change, which may allow ferruginous indurations to be applied as a novel tool to yield absolute age constraints on arid landscape evolution globally. Age constraints on such induration features that are interpreted to capture changing hydrological and redox conditions in line with a global climatic change, may have the potential to significantly aid temporal understanding of aridification and hydrological processes on a local to global scale. Importantly, ferruginous indurations are frequently recognized in regolith and sediments across Australia (Anand & Paine, 2002; Chan, 2009; Heim et al., 2006; Worrall, 2017) and globally (Nahon et al., 1977; Ricordel-Prognon et al., 2010; Voicu et al., 1997). Ultimately, absolute age constraints associated with direct

terrestrial products of climatic transitions could plausibly provide vital anchor points for the understanding of the coevolution of landscapes and biota.

Data Availability Statement

All new research data used in this publication and detailed analytical methods are deposited in the Dryad and Zenodo repositories. Supporting Information S1 is available through Zenodo (https://doi.org/10.5281/zenodo.7739575) and includes Texts S1–S4, Figures S1 and S2, and Tables S1–S3. Tables S4 and S5 are available through Dryad (https://doi.org/10.5061/dryad.sn02v6x86). Literature data for this research are available in Christensen et al. (2017), Cramer et al. (2011), Hanesch (2009), Lisiecki and Raymo (2005), K. G. Miller et al. (2020), Smith et al. (2020), and Woodhead et al. (2019). Past 4.03 software (Hammer et al., 2001), used for the Epps-Singelton test, is available through https://www.nhm.uio.no/english/research/resources/past/; Probability density plots were constructed using Excel macros available through the Arizona LaserChron Center (https://drive.google.com/file/d/1ju5B_h4kHvb-K7PR2WHM9DJQELByqdJP_/view); Weighted mean calculation and outlier detection were performed using IsoplotR (Vermeesch, 2018) available through https://www.ucl.ac.uk/~ucfbpve/isoplotr/home/index.html; Raman spectra background subtraction and averaging was performed in Fityk available through https://fityk.nieto.pl/.

Acknowledgments
This research was supported by Minerals Research Institute of Western Australia Grant M551. We thank Rohan Hine and David Sleigh of Iluka Resources for discussions and sample material. Sarah Feakins is thanked for editorial handling. Cécile Gautheron and two anonymous reviewers are thanked for thoughtful and constructive comments that improved this contribution. Open access publishing facilitated by Curtin University, as part of the Wiley - Curtin University agreement via the Council of Australian University Librarians.

References

Anand, R. R., & Paine, M. (2002). Regolith geology of the Yilgarn Craton, Western Australia: Implications for exploration. *Australian Journal of Earth Sciences*, *49*(1), 3–162. https://doi.org/10.1046/j.1440-0952.2002.00912.x

Ansari, M. H., Cooper, S. J. B., Schwarz, M. P., Ebrahimi, M., Dolman, G., Reinberger, L., et al. (2019). Plio-Pleistocene diversification and biogeographic barriers in southern Australia reflected in the phylogeography of a widespread and common lizard species. *Molecular Phylogenetics and Evolution*, *133*, 107–119. https://doi.org/10.1016/j.ympev.2018.12.014

Bailey, I., Hole, G. M., Foster, G. L., Wilson, P. A., Storey, C. D., Trueman, C. N., & Raymo, M. E. (2013). An alternative suggestion for the Pliocene onset of major northern hemisphere glaciation based on the geochemical provenance of North Atlantic Ocean ice-rafted debris. *Quaternary Science Reviews*, *75*, 181–194. https://doi.org/10.1016/j.quascirev.2013.06.004

Balco, G., & Rovey, C. W. (2010). Absolute chronology for major Pleistocene advances of the Laurentide Ice Sheet. *Geology*, *38*(9), 795–798. https://doi.org/10.1130/g30946.1

Bassal, F., Heller, B., Roques, J., Balout, H., Tassan-Got, L., Allard, T., & Gautheron, C. (2022). Revealing the radiation damage and Al-content impacts on He diffusion in goethite. *Chemical Geology*, *611*, 121118. https://doi.org/10.1016/j.chemgeo.2022.121118

Bigham, J. M., Fitzpatrick, R. W., & Schulze, D. G. (2002). Iron oxides. In J. B. Dixon & D. G. Schulze (Eds.), *SSSA book series: Vol. 7. Soil mineralogy with environmental applications* (pp. 323–366). John Wiley & Sons, Ltd.

Byrne, M., Yeates, D. K., Joseph, L., Kearney, M., Bowler, J., Williams, M. A. J., et al. (2008). Birth of a biome: Insights into the assembly and maintenance of the Australian arid zone biota. *Molecular Ecology*, *17*(20), 4398–4417. https://doi.org/10.1111/j.1365-294X.2008.03899.x

Chan, R. A. (2009). Evolution of the Girilambone regolith landscape, central-western New South Wales. *Australian Journal of Earth Sciences*, *56*(sup1), S105–S123. https://doi.org/10.1080/08120090902871135

Christensen, B. A., Renema, W., Henderiks, J., Vleeschouwer, D., de Groeneveld, J., Castañeda, I. S., et al. (2017). Indonesian Throughflow drove Australian climate from humid Pliocene to arid Pleistocene. *Geophysical Research Letters*, *44*(13), 6914–6925. https://doi.org/10.1002/2017GL072977

Courtillat, M., Hallenberger, M., Bassetti, M.-A., Aubert, D., Jeandel, C., Reuning, L., et al. (2020). New record of dust input and provenance during glacial periods in Western Australia Shelf (IODP expedition 356, site U1461) from the Middle to Late Pleistocene. *Atmosphere*, *11*(11), 1251. https://doi.org/10.3390/atmos11111251

Cramer, B. S., Miller, K. G., Barrett, P. J., & Wright, J. D. (2011). Late Cretaceous–Neogene trends in deep ocean temperature and continental ice volume: Reconciling records of benthic foraminiferal geochemistry ($\delta^{18}O$ and Mg/Ca) with sea level history. *Journal of Geophysical Research*, *116*(C12), C12023. https://doi.org/10.1029/2011JC007255

Crisp, M. D., & Cook, L. G. (2007). A congruent molecular signature of vicariance across multiple plant lineages. *Molecular Phylogenetics and Evolution*, *43*(3), 1106–1117. https://doi.org/10.1016/j.ympev.2007.02.030

Danišík, M., Evans, N. J., Ramanaidou, E. R., McDonald, B. J., Mayers, C., & McInnes, B. I. A. (2013). (U–Th)/He chronology of the Robe River channel iron deposits, Hamersley Province, Western Australia. *Chemical Geology*, *354*, 150–162. https://doi.org/10.1016/j.chemgeo.2013.06.012

Danišík, M., McInnes, B. I. A., Kirkland, C. L., McDonald, B. J., Evans, N. J., & Becker, T. (2017). Seeing is believing: Visualization of He distribution in zircon and implications for thermal history reconstruction on single crystals. *Science Advances*, *3*(2), e1601121. https://doi.org/10.1126/sciadv.1601121

DeMenocal, P. B. (2011). Anthropology. Climate and human evolution. *Science*, *331*(6017), 540–542. https://doi.org/10.1126/science.1190683

de Vleeschouwer, D., Petrick, B. F., & Martínez-García, A. (2019). Stepwise weakening of the Pliocene Leeuwin current. *Geophysical Research Letters*, *46*(14), 8310–8319. https://doi.org/10.1029/2019GL083670

Epps, T. W., & Singleton, K. J. (1986). An omnibus test for the two-sample problem using the empirical characteristic function. *Journal of Statistical Computation and Simulation*, *26*(3–4), 177–203. https://doi.org/10.1080/00949658608810963

Filippelli, G. M., & Flores, J.-A. (2009). From the warm Pliocene to the cold Pleistocene: A tale of two oceans. *Geology*, *37*(10), 959–960. https://doi.org/10.1130/focus102009.1

Fujioka, T., Chappell, J., Fifield, L. K., & Rhodes, E. J. (2009). Australian desert dune fields initiated with Pliocene–Pleistocene global climatic shift. *Geology*, *37*(1), 51–54. https://doi.org/10.1130/g25042a.1

Gautheron, C., Sawakuchi, A. O., dos Santos Albuquerque, M. F., Cabriolu, C., Parra, M., Ribas, C. C., et al. (2022). Cenozoic weathering of fluvial terraces and emergence of biogeographic boundaries in Central Amazonia. *Global and Planetary Change*, *212*, 103815. https://doi.org/10.1016/j.gloplacha.2022.103815

Groeneveld, J., De Vleeschouwer, D., McCaffrey, J. C., & Gallagher, S. J. (2021). Dating the northwest shelf of Australia since the Pliocene. *Geochemistry, Geophysics, Geosystems*, *22*, e2020GC009418. https://doi.org/10.1029/2020GC009418

Guyodo, Y., Mostrom, A., Lee Penn, R., & Banerjee, S. K. (2003). From nanodots to nanorods: Oriented aggregation and magnetic evolution of nanocrystalline goethite. *Geophysical Research Letters*, *30*(10), n/a. https://doi.org/10.1029/2003GL017021

Hammer, Ø., Harper, D. A. T., & Ryan, P. D. (2001). PAST: Paleontological statistics software package for education and data analysis. *Palaeontologia Electronica*, *4*(1), 9. http://palaeo-electronica.org/2001_1/past/issue1_01.htm

Hanesch, M. (2009). Raman spectroscopy of iron oxides and (oxy)hydroxides at low laser power and possible applications in environmental magnetic studies. *Geophysical Journal International*, *177*(3), 941–948. https://doi.org/10.1111/j.1365-246X.2009.04122.x

Haug, G. H., Sigman, D. M., Tiedemann, R., Pedersen, T. F., & Sarnthein, M. (1999). Onset of permanent stratification in the subarctic Pacific Ocean. *Nature*, *401*(6755), 779–782. https://doi.org/10.1038/44550

He, Y., Wang, H., & Liu, Z. (2021). Development of the Leeuwin current on the northwest shelf of Australia through the Pliocene-Pleistocene period. *Earth and Planetary Science Letters*, *559*, 116767. https://doi.org/10.1016/j.epsl.2021.116767

Heim, J. A., Vasconcelos, P. M., Shuster, D. L., Farley, K. A., & Broadbent, G. (2006). Dating paleochannel iron ore by (U-Th)/He analysis of supergene goethite, Hamersley province, Australia. *Geology*, *34*(3), 173–176. https://doi.org/10.1130/g22003.1

Hill, D. J., Bolton, K. P., & Haywood, A. M. (2017). Modelled ocean changes at the Plio-Pleistocene transition driven by Antarctic ice advance. *Nature Communications*, *8*(1), 14376. https://doi.org/10.1038/ncomms14376

Hou, B., Keeling, J., Reid, A., Fairclough, M., Warland, I., Belousova, E., et al. (2011). Heavy mineral sands in the Eucla Basin, southern Australia: Deposition and province-scale prospectivity. *Economic Geology*, *106*(4), 687–712. https://doi.org/10.2113/econgeo.106.4.687

IGS. (2019). Jacinth-Ambrosia mine groundwater model update. A report prepared for Iluka Resources Limited.

Lipar, M., & Ferk, M. (2015). Karst pocket valleys and their implications on Pliocene–Quaternary hydrology and climate: Examples from the Nullarbor Plain, southern Australia. *Earth-Science Reviews*, *150*, 1–13. https://doi.org/10.1016/j.earscirev.2015.07.002

Lisiecki, L. E., & Raymo, M. E. (2005). A Pliocene-Pleistocene stack of 57 globally distributed benthic $\delta^{18}O$ records. *Paleoceanography*, *20*(1), PA1003. https://doi.org/10.1029/2004PA001071

Lisiecki, L. E., & Raymo, M. E. (2007). Plio–Pleistocene climate evolution: Trends and transitions in glacial cycle dynamics. *Quaternary Science Reviews*, *26*(1–2), 56–69. https://doi.org/10.1016/j.quascirev.2006.09.005

Martin, H. A. (2006). Cenozoic climatic change and the development of the arid vegetation in Australia. *Journal of Arid Environments*, *66*(3), 533–563. https://doi.org/10.1016/j.jaridenv.2006.01.009

Miller, C. R., James, N. P., & Bone, Y. (2012). Prolonged carbonate diagenesis under an evolving late Cenozoic climate; Nullarbor Plain, southern Australia. *Sedimentary Geology*, *261–262*, 33–49. https://doi.org/10.1016/j.sedgeo.2012.03.002

Miller, K. G., Browning, J. V., Schmelz, W. J., Kopp, R. E., Mountain, G. S., & Wright, J. D. (2020). Cenozoic sea-level and cryospheric evolution from deep-sea geochemical and continental margin records. *Science Advances*, *6*(20), eaaz1346. https://doi.org/10.1126/sciadv.aaz1346

Mirzabaev, A., Wu, J., Evans, J., García-Oliva, F., Hussein, I. A. G., Iqbal, M. H., et al. (2019). Desertification. In P. R. Shukla, J. Skea, E. Calvo Buendia, V. Masson-Delmotte, H.-O. Pörtner, D. C. Roberts, et al. (Eds.), *Climate change and land: An IPCC special report on climate change, desertification, land degradation, sustainable land management, food security, and greenhouse gas fluxes in terrestrial ecosystems*. Cambridge University Press. https://doi.org/10.1017/9781009157988.005

Nahon, D. (1991a). *Introduction to the petrology of soils and chemical weathering*. Wiley.

Nahon, D. (1991b). Self-organization in chemical lateritic weathering. *Geoderma*, *51*(1–4), 5–13. https://doi.org/10.1016/0016-7061(91)90063-Y

Nahon, D., Janot, C., Karpoff, A. M., Paquet, H., & Tardy, Y. (1977). Mineralogy, petrography and structures of iron crusts (ferricretes) developed on sandstones in the western part of Senegal. *Geoderma*, *19*(4), 263–277. https://doi.org/10.1016/0016-7061(77)90069-6

Owen, C. L., Marshall, D. C., Hill, K. B. R., & Simon, C. (2017). How the aridification of Australia structured the biogeography and influenced the diversification of a large lineage of Australian cicadas. *Systematic Biology*, *66*(4), 569–589. https://doi.org/10.1093/sysbio/syw078

Pepper, M., & Keogh, J. S. (2021). Life in the "dead heart" of Australia: The geohistory of the Australian deserts and its impact on genetic diversity of arid zone lizards. *Journal of Biogeography*, *48*(4), 716–746. https://doi.org/10.1111/jbi.14063

Petrick, B., Martínez-García, A., Auer, G., Reuning, L., Auderset, A., Deik, H., et al. (2019). Glacial Indonesian Throughflow weakening across the Mid-Pleistocene climatic transition. *Scientific Reports*, *9*(1), 16995. https://doi.org/10.1038/s41598-019-53382-0

Reed, K. E. (1997). Early hominid evolution and ecological change through the African Plio-Pleistocene. *Journal of Human Evolution*, *32*(2–3), 289–322. https://doi.org/10.1006/jhev.1996.0106

Reid, N., Gray, D. J., Wilson, T., Reid, A., Petts, A., de Caritat, P., & Thorne, R. (2018). *Hydrogeochemical atlas of South Australia*. CSIRO.

Reiners, P. W., & Nicolescu, S. (2006). Measurement of parent nuclides for (U–Th)/He chronometry by solution sector ICP-MS. *ARHDL Report*, *1*, 1–33.

Ricordel-Prognon, C., Lagroix, F., Moreau, M.-G., & Thiry, M. (2010). Lateritic paleoweathering profiles in French Massif Central: Paleomagnetic datings. *Journal of Geophysical Research*, *115*(B10), B10104. https://doi.org/10.1029/2010JB007419

Rix, M. G., Edwards, D. L., Byrne, M., Harvey, M. S., Joseph, L., & Roberts, J. D. (2015). Biogeography and speciation of terrestrial fauna in the south-western Australian biodiversity hotspot. *Biological Reviews of the Cambridge Philosophical Society*, *90*(3), 762–793. https://doi.org/10.1111/brv.12132

Salama, W., Anand, R. R., Tunmer, W., & Aspandiar, M. (2022). Regolith characterization and landscape evolution for geochemical exploration of the covered Yamarna Terrane, Western Australia. *Journal of Geochemical Exploration*, *232*, 106881. https://doi.org/10.1016/j.gexplo.2021.106881

Schwertmann, U., & Taylor, R. M. (1989). Iron oxides. In J. B. Dixon & S. B. Weed (Eds.), *Minerals in soil environments*. John Wiley & Sons, Ltd. https://doi.org/10.2136/sssabookser1.2ed.c8

Seltzer, A. M., Ng, J., Danskin, W. R., Kulongoski, J. T., Gannon, R. S., Stute, M., & Severinghaus, J. P. (2019). Deglacial water-table decline in Southern California recorded by noble gas isotopes. *Nature Communications*, *10*(1), 5739. https://doi.org/10.1038/s41467-019-13693-2

Shuster, D. L., Vasconcelos, P. M., Heim, J. A., & Farley, K. A. (2005). Weathering geochronology by (U-Th)/He dating of goethite. *Geochimica et Cosmochimica Acta*, *69*(3), 659–673. https://doi.org/10.1016/j.gca.2004.07.028

Smith, R. A., Castañeda, I. S., Groeneveld, J., de Vleeschouwer, D., Henderiks, J., Christensen, B. A., et al. (2020). Plio-Pleistocene Indonesian Throughflow variability drove eastern Indian Ocean sea surface temperatures. *Paleoceanography and Paleoclimatology*, *35*(10). https://doi.org/10.1029/2020PA003872

Sniderman, J. K., Woodhead, J. D., Hellstrom, J., Jordan, G. J., Drysdale, R. N., Tyler, J. J., & Porch, N. (2016). Pliocene reversal of late Neogene aridification. *Proceedings of the National Academy of Sciences*, *113*(8), 1999–2004. https://doi.org/10.1073/pnas.1520188113

Torrent, J., Guzman, R., & Parra, M. A. (1982). Influence of relative humidity on the crystallization of Fe (III) oxides from ferrihydrite. *Clays and Clay Minerals*, *30*(5), 337–340. https://doi.org/10.1346/ccmn.1982.0300503

Trauth, M. H., Asrat, A., Berner, N., Bibi, F., Foerster, V., Grove, M., et al. (2021). Northern hemisphere glaciation, African climate and human evolution. *Quaternary Science Reviews*, *268*, 107095. https://doi.org/10.1016/j.quascirev.2021.107095

Van der Esch, S., ten Brink, B., Stehfest, E., Bakkenes, M., Sewell, A., Bouwman, A., et al. (2017). *Exploring future changes in land use and land condition and the impacts on food, water, climate change and biodiversity: Scenarios for the UNCCD Global Land Outlook*. PBl Netherlands Environmental Assessment Agency.

Vermeesch, P. (2018). IsoplotR: A free and open toolbox for geochronology. *Geoscience Frontiers*, *9*(5), 1479–1493. https://doi.org/10.1016/j.gsf.2018.04.001

Voicu, G., Bardoux, M., & Voicu, D. (1997). Mineralogical norm calculations applied to tropical weathering profiles. *Mineralogical Magazine*, *61*(405), 185–196. https://doi.org/10.1180/minmag.1997.061.405.03

Webb, J. A., & James, J. M. (2006). Karst evolution of the Nullarbor plain, Australia. *Special Paper of the Geological Society of America*, *404*, 65.

White, N. E., Phillips, M. J., Gilbert, M. T. P., Alfaro-Núñez, A., Willerslev, E., Mawson, P. R., et al. (2011). The evolutionary history of cockatoos (Aves: Psittaciformes: Cacatuidae). *Molecular Phylogenetics and Evolution*, *59*(3), 615–622. https://doi.org/10.1016/j.ympev.2011.03.011

Woodhead, J. D., Sniderman, J. M. K., Hellstrom, J., Drysdale, R. N., Maas, R., White, N., et al. (2019). The antiquity of Nullarbor speleothems and implications for karst palaeoclimate archives. *Scientific Reports*, *9*(1), 603. https://doi.org/10.1038/s41598-018-37097-2

Worrall, L. (2017). Exploring for heavy minerals on Cape York Peninsula, Queensland, Australia. *Australian Journal of Earth Sciences*, *64*(8), 1055–1071. https://doi.org/10.1080/08120099.2017.1380700

Yee, N., Shaw, S., Benning, L. G., & Nguyen, T. H. (2006). The rate of ferrihydrite transformation to goethite via the Fe(II) pathway. *American Mineralogist*, *91*(1), 92–96. https://doi.org/10.2138/am.2006.1860

Zhao, L., Hong, H., Fang, Q., Yin, K., Wang, C., Li, Z., et al. (2017). Monsoonal climate evolution in southern China since 1.2 Ma: New constraints from Fe-oxide records in red Earth sediments from the Shengli section, Chengdu Basin. *Palaeogeography, Palaeoclimatology, Palaeoecology*, *473*, 1–15. https://doi.org/10.1016/j.palaeo.2017.02.027

Zomer, R. J., Trabucco, A., Bossio, D. A., & Verchot, L. V. (2008). Climate change mitigation: A spatial analysis of global land suitability for clean development mechanism afforestation and reforestation. *Agriculture, Ecosystems & Environment*, *126*(1–2), 67–80. https://doi.org/10.1016/j.agee.2008.01.014